Material parameters for shell zones made of crystalline rock derived from measurement

M. Holzmann[1], S. Perzlmaier[1] and B. Hofer[1]

[1] TIWAG-Tiroler Wasserkraft AG, Eduard-Wallnöfer-Platz 2, A-6020 Innsbruck, Austria

E-mail: michael.holzmann@tiwag.at

Summary

The derivation of material parameters for shell zones presented in this paper is mainly based on measurements during construction and operation of Gepatsch and Finstertal dam. The analyzed data originate from surface points (three dimensional deformation), horizontal and vertical extensometers (longitudinal deformation) as well as inclinometers (inclination), strain measurement devices (two dimensional) and earth pressure cells (total stress) combined with piezometers (effective stress). The presented stress strain curves for crystalline rockfill and fill from well graded moraine material consider initial deformation until the end of construction, saturation settlements in the upstream shell zone during first filling and draw down as well as time depended settlements caused by creep effects.

The paper gives a retrospective of how the stress-strain relation for the shell zones of Finstertal rockfill dam was derived and describes an advanced technique to determine material parameters for the nonlinear Hardening Soil model. Results from finite element computations based on these physically derived material parameters give very good accordance with deformation behaviour as well as the stress distribution of Finstertal dam.

Introduction

Numerical analysis in dam engineering is common practice since decades. In the very beginnings computations were limited by computing capacity and material models which could not describe the behaviour of soil sufficiently. More sophisticated constitutive models as well as program applications have been developed over time and made the prediction of dam behaviour more realistic. The quality of finite element computations to predict the stress strain characteristics and deformation pattern of the dam body for several load cases depends on several issues such as discretization, material model and particularly the quality of the input data. The calibration of numerical model parameters is usually based on laboratory tests such as triaxial and/or oedometer tests. Those tests are often limited in terms of maximum grain size.

Alternatively, material parameters can be determined by evaluating the stress strain behaviour of existing dams on the basis of deformation and stress measurement. Those measurements of TIWAG's Gepatsch and Finstertal dam were the basis for the derivation and evaluation of nonlinear stress strain relations for shell zones made of moraine and rockfill material. This stress strain curves are the basis for the calibration of material parameters and have been verified by a finite element computation of Finstertal dam. The presented material parameter set seems to be well suitable for the computation of future dam projects with similar geotechnical conditions.

Finstertal rockfill dam

The 150 m high Finstertal dam was built in 1977-1980. Due to morphological and geotechnical conditions an asphaltic concrete rockfill dam proved to be the best solution. The main dam cross section and its zoning are pictured in Figure 1.

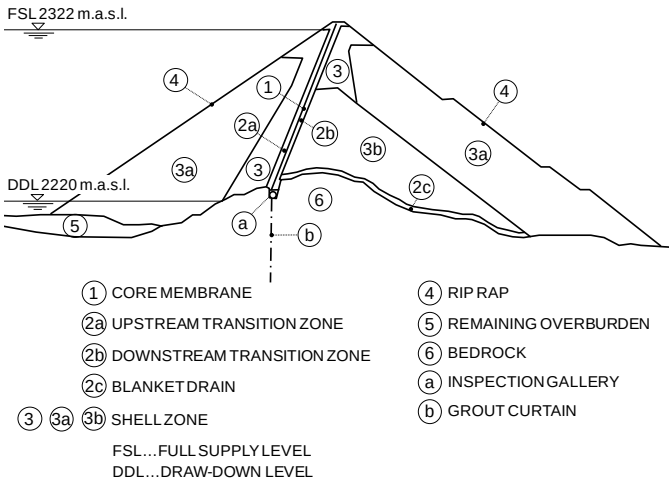

Figure 1: Finstertal rockfill dam

Construction

The asphaltic concrete core is founded on an inspection and grouting gallery made of cast-in-place concrete which is built in polymetamorphic gneiss. The thickness of the core decreases from 70 cm at its base to 50 cm at the crest. The

core was placed with an inclination of 1 to 0.4 and follows a rock shoulder in longitudinal direction. In the upstream shell rockfill material (3, 3a, granodiorite) was placed, in the downstream shell moraine material (3b). Core and adjacent zones (2a, 2b) were placed in 25 cm layers and compacted simultaneously. To optimize layer thickness and maximum grain size of the shell zones large scale compaction tests were carried out prior to the fill works. Layer thicknesses as well as number of passes of a 15 tons vibrating roller compactor were varied along test fields to determine the optimum regarding constructional and economical aspects. Figure 2 shows the compaction success in terms of porosity for quarried granodiorite rockfill for different layer thicknesses and numbers of passes. The in situ tests pointed out that the compaction success is mainly depended on the placed layer thickness.

Similar experience was made in the compaction tests with moraine material (3b), although, the number of passes should be more relevant.

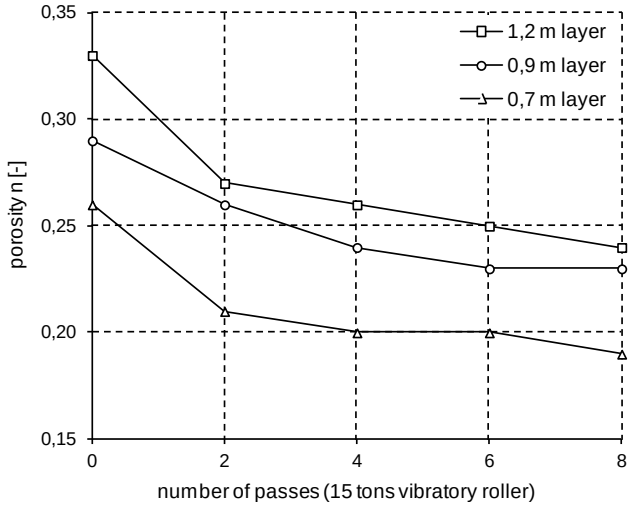

Figure 2: Compression of soil as a function of layer thickness and compaction effort gained from large scale compaction tests on granodiorite rockfill

A layer thickness of 100 cm, a maximum particle size (MPS) of 700 mm and 6 passes were selected for the upstream and downstream shell zones (3a and 3b). To increase fill density and stiffness in a close range to the asphaltic concrete core the layer thickness of the quarry run rockfill material was reduced to 75 cm in zone 3. The ranges of particle size graduation curves for the various dam zones are pictured in Figure 3. The upstream shell zone was wetted with 0.5 m³ of water per 1 m³ of rockfill to partly anticipate saturation settlements which may occur in embankment dams made of quarried rock during first impoundment [9]. The mean porosity is 24% in the rockfill zone 3a and 18% in the moraine material zone 3b, respectively [7].

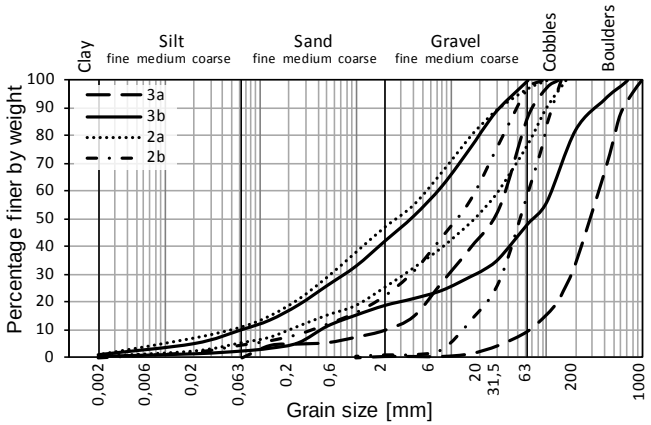

Figure 3: Ranges of particle size graduation curves for Finstertal dam zones

Extensive testing of the compacted fill as well as in the onsite geotechnical laboratory displays the quality of the fill materials and the construction works. The geotechnical specifications (MPS, layer thickness) defined prior to construction as well as the mean placement values for the dam zones (n, γ) are listed in Table 1.

TABLE 1: SPECIFICATION OF DAM ZONES

ZONE	MATERIAL	MPS [mm]	LAYER THICKNESS [cm]	MEAN POROSITY n [%]	MEAN FILL DENSITY γ [kN/m³]
1	asphalt	16	25	< 2	23,94
2a	sieved moraine	100	25	20	23,15
2b	sieved rockfill	100	25	24	21,19
2c	rockfill	700	100	23,5	20,89
3	rockfill	700	75	21	21,78
3a	rockfill	700	100	24	20,89
3b	moraine	700	100	18	23,64
4	rockfill	1000	--	--	
5	moraine	--	--	22	23,50

Deformations at the end of construction

The effort made in design and construction lead to a excellent deformation behaviour of the dam. The maximum settlement at the end of construction was located in the downstream shell zone 3a and reached a value of about 30 cm (Figure 14). The maximum horizontal displacement of 13 cm was located half way up in the upstream shell. The horizontal displacement on the same level in the downstream shell was maximum 10 cm [7].

Behaviour during first impoundment and drawdown

The additional load from reservoir filling is transferred into the downstream bedrock by the well-graded moraine material

zone 3b with a very low porosity and therefore a rather high stiffness and strength. Settlement in the downstream shell zone increased after first filling and drawdown by 10 cm compared to the end of construction stage. The first filling caused horizontal displacements with a maximum of 14 cm at the crest, which partly moved backward during first drawdown.
As an effect of additional loading and ongoing consolidation the porosity of the moraine material zone 3b decreased from 18% to 16.5% and for the rockfill zone 3 from 24% to 23% until the first drawdown.

Derivation of deformation characteristics

The basic procedure to evaluate stress strain characteristics for the shell zones of Finstertal rockfill dam was derived by analyzing the deformation pattern and stress redistribution characteristics of Gepatsch rockfill dam for the end of construction stage and after 14 years of operation. Both, Finstertal and Gepatsch rockfill dam were built in the same crystalline rock mass and the shell zones are made of similar rockfill material (orthogneiss) with comparable rock mechanical properties. Apart from the dam type (Gepatsch is a central earth core dam), the main difference lies in the placement and compaction effort of the shell zones. The rockfill of Gepatsch dam, built in the early 1960s, was placed in 2 m layers (MPS 1500 mm) and compacted by 8.5 tons vibratory rollers. Thus, the initial mean fill porosity of 28.8% was much higher compared to modern thin layer compaction (for example 24% at Finstertal dam) [6]. The maximum settlements at the end of construction lied in a range of 2.5 m located in the middle of the shell zones. The deformation characteristic and stress distribution pattern for Gepatsch dam was derived from earth pressure and internal displacement measurement [10]. The findings from Gepatsch rockfill dam, concerning the decrease of porosity and increase of stiffness over time had been transferred to predict the deformation behaviour of Finstertal dam. The difference in the initial porosity of the placed rockfill layers between Finstertal and Gepatsch was 4.8%. By considering the deformations of Gepatsch rockfill dam due to consolidation to the same porosity and fill density as Finstertal dam after the end of construction, a reference state was determined to predict long time behaviour in analogy to Gepatsch dam.
The bearing behaviour of Finstertal dam was measured in six dam cross sections and in longitudinal direction by internal and external deformation measurement and special strain measurement devices (Figure 4). Stresses were measured at 102 earth pressure cells arranged in three dimensions, carefully installed to minimize stress redistribution due to the differential stiffness of the layered soil and the pressure cells. The measured data was verified and optimized with calibrated data sets determined prior under laboratory conditions [8].

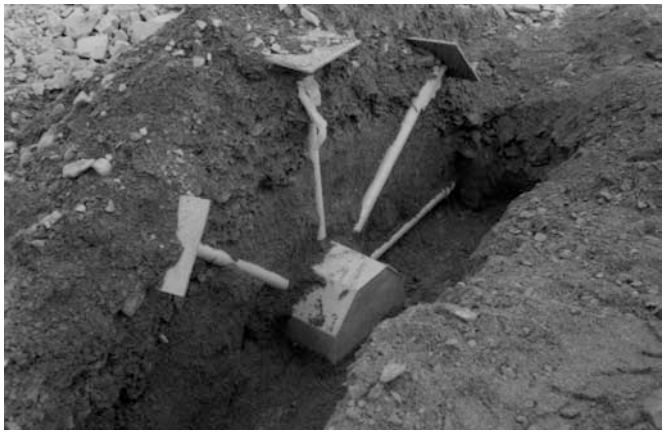

Figure 4: Strain measurement device embedded in moraine material zone 3b

The basis for the derivation of stress strain curves for the shell zones of Finstertal rockfill dam for the load cases end of construction, first filling/drawdown and after 15 years of operation was the generation of stress and strain states from measurement data. Schwab [8] started with the elaboration of stress and strain distribution patterns for the main dam cross section. The distribution and the direction of principal stress and principal strain were used to generate ($\sigma_1 - \sigma_3$) over ε_1 curves for several minor principle stress states σ_3 in a second step (Figure 5 and 6).

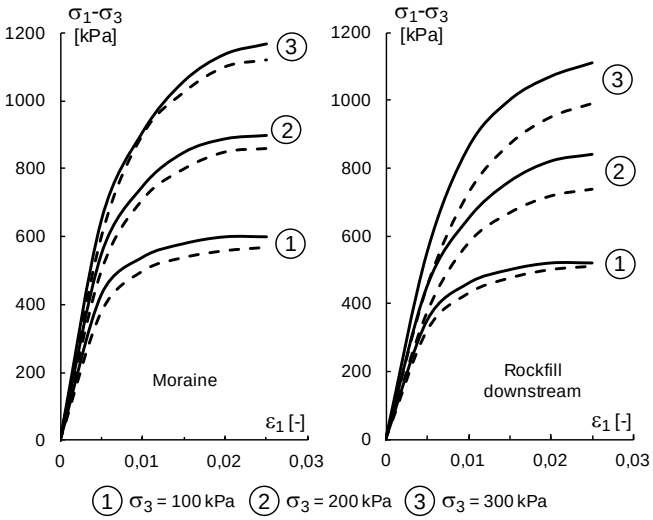

Figure 5: Stress strain curves for moraine material zone 3b (left) and downstream rockfill zone 3, 3a (right) for the end of construction stage (continuous line) and after 15 years of operation (slashed line)

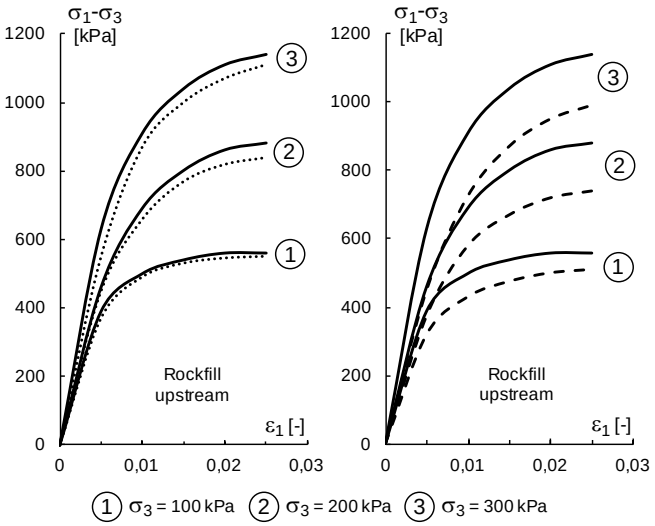

Figure 6: Stress strain curves for upstream rockfill zone 3, 3a for the end of construction stage (continuous line), after first impoundment (dashed line, left) and after 15 years of operation (slashed line, right)

Constitutive modelling

Hardening Soil constitutive model

The procedure to determine material parameters for the Hardening Soil model was enhanced by the authors. It combines the standard procedure mentioned by Schanz et al. [5] with the formulation of initial soil stiffness after Kondner [2]. The modified method derives the crucial ratio R_f from stress strain curves instead of estimating it.

The nonlinear stress strain characteristic of the soil is approximated by a hyperbolic function based on a formulation by Kondner and his co-workers which is also used in the elastic stiffness formulation of the Duncan-Chang model. The nonlinear approach in Equation (1) is a function of the major and minor principle stress and the axial strain.

$$(\sigma_1 - \sigma_3) = \frac{\varepsilon_1}{a + b\varepsilon_1} \qquad (1)$$

The value of a is the reciprocal of the initial tangent stiffness E_i and b is the reciprocal of the theoretical stress difference q_a at infinite axial strain (Figure 7) [2].

The advantages of the Hardening Soil model compared to the widespread Duncan-Chang model are the formulation in terms of plasticity rather than elasticity, the modelling of soil dilation and the formulation of yield functions. Distinctions are made between shear hardening, modelling plastic strains due to primary deviatoric loading, and compression hardening modelling plastic strains due to primary compression loading. For that purpose a shear yield surface and a cap yield surface which expand in the principal stress space are formulated to independently describe both phenomena. A summary and description of basic Hardening Soil parameters can be found in Table 2 and [5].

TABLE 2: BASIC HARDENING SOIL PARAMETERS

Stiffness parameters	
$E_{50,ref}$	: reference secant stiffness modulus
$E_{oed,ref}$	: reference tangent stiffness for primary oedometer loading
$E_{ur,ref}$	: reference young's modulus for unloading/reloading
m	: power m for stress level dependency of stiffness
σ_3'	: (effective) minor principal stress; positive for compression
K_0^{nc}	: K_0-value for normal consolidation (K_0^{nc} = 1-sinφ)
Strength parameters	
c	: effective cohesion
φ	: effective friction angle
ψ	: angle of dilatancy
R_f	: failure ratio

The stiffness parameters $E_{50,ref}$, $E_{oed,ref}$ and $E_{ur,ref}$ correspond to a reference stress p_{ref} at 100 kPa and are the basis for the formulation of the stress depended stiffness Equations (2), (5) and (6). The stiffness equations in the Hardening Soil model are formulated as a function of the minor principal stress σ_3. The nonlinear primary behaviour for drained triaxial stiffness E_{50} is modelled by Equation (2).

$$E_{50} = E_{50,ref}\left[\frac{c\cdot\cos\varphi + \sigma_3'\cdot\sin\varphi}{c\cdot\cos\varphi + p^{ref}\cdot\sin\varphi}\right]^m = E_{50,ref}[K]^m \qquad (2)$$

The reference stiffness modulus for shear loading $E_{50,ref}$ controls the magnitude of the plastic shear strains and is determined from the initial stiffness E_i by Equation (3) [4].

$$E_{50} = \frac{E_i\cdot(2-R_f)}{2} \qquad (3)$$

The factor R_f after Kondner defines the ratio of the deviatoric stress at failure q_f and the asymptotic value q_a of the hyperbolic stress strain function:

$$R_f = \frac{q_f}{q_a}. \qquad (4)$$

In the elasto-plastic Hardening Soil model no relationship is formulated between E_{50} and E_{oed}. The oedometer stiffness E_{oed} is given independently by:

$$E_{oed} = E_{oed,ref}\left[\frac{c\cdot\cos\varphi + \frac{\sigma_3'}{K_0^{nc}}\cdot\sin\varphi}{c\cdot\cos\varphi + p^{ref}\cdot\sin\varphi}\right]^m. \qquad (5)$$

The reference stiffness modulus for isotropic compression $E_{oed,ref}$ controls the magnitude of plastic strains (compression yield cap).
For modelling unloading/reloading behaviour a separate stress depended stiffness modulus is used:

$$E_{ur} = E_{ur,ref}\left[\frac{c\cdot\cos\varphi + \sigma_3'\cdot\sin\varphi}{c\cdot\cos\varphi + p^{ref}\cdot\sin\varphi}\right]^m. \qquad (6)$$

The stiffness parameters for the Hardening Soil model are illustrated in Figure 7.

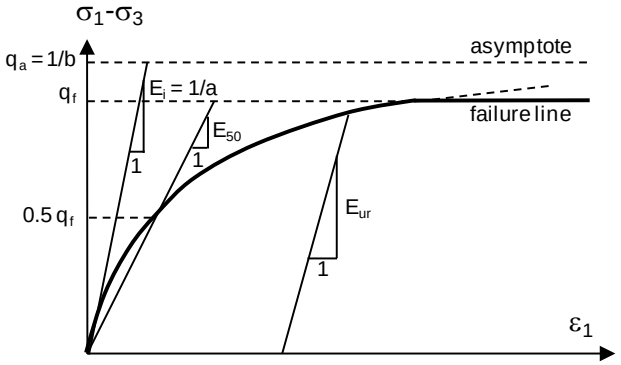

Figure 7: Hyperbolic stress strain relation under drained triaxial conditions [5]

Dilation is modelled by the angle of ψ. The strength parameters coincide with those of the Mohr-Coulomb model.
All parameters used in the Hardening Soil model have physical equivalence and can therefore be determined from laboratory tests or otherwise generated stress strain curves.

Applied technique for parameter determination
The data for which the material parameters are evaluated should be appropriate to the problem being analyzed. In case of dam fill materials, the laboratory tests should be specified using specimens compacted to the same density and water content as in the field. The stress state for which the stress strain curves are generated should be representative for the conditions within the embankment. Stress strain curves derived from existing dams have to fulfil the same requirements. At least three stress strain curves for different confining pressures σ_3 should be used to evaluate the material parameters [3].
The procedure for the evaluation of the Hardening Soil stiffness parameters $E_{50,ref}$, the power value m and the failure ratio R_f is illustrated in Figure 9 and 10 using the stress strain curves in Figure 8. It is known from comparative calculations by the authors that the best match for the hyperbola to the stress strain curve is achieved by selecting data points at 40%, 70% and 95% of deviatoric stress at failure q_f (Mohr-Coulomb strength).

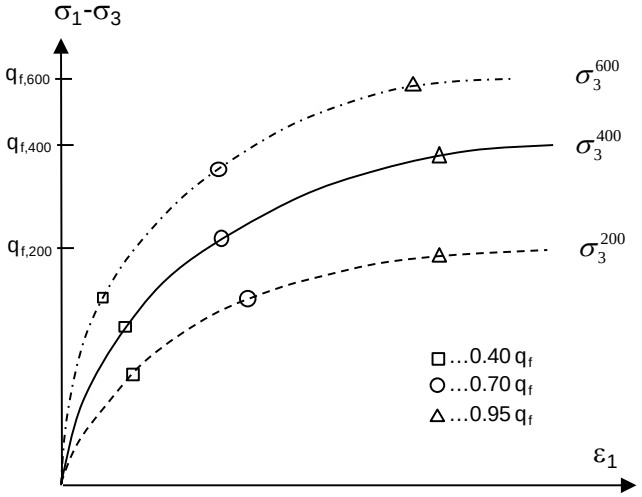

Figure 8: Selected data points for model calibration at 40%, 70% and 95% of strength q_f

The specified data points are plotted in a transformed linearized form of Equation (1). From the $\varepsilon_1/(\sigma_1-\sigma_3)$ over ε_1 diagram the initial stiffness E_i as well as the theoretical asymptotic value q_a can be calculated as the reciprocal of the y-intercept and the reciprocal of the slope of the regression line (Figure 9).

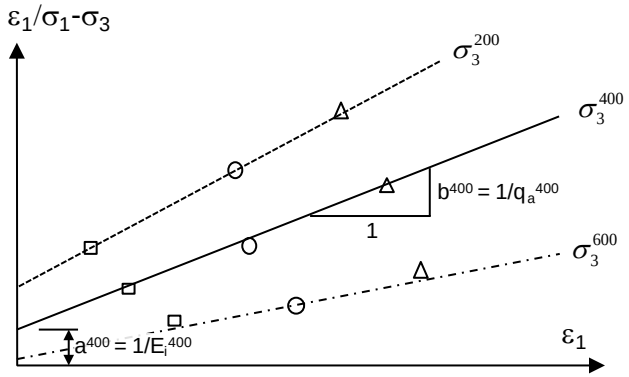

Figure 9: Determination of initial stiffness E_i and asymptotic value q_a after linearization of Equation (1)

The failure ratio R_f and the stiffness modulus E_{50} depend on the minor principal stress σ_3 and may be computed by Equations (4) and (2). The reference stiffness modulus $E_{50,ref}$ corresponding to a minor principal stress $\sigma_3 = p_{ref} = 100$ kPa and the power value m is determined by plotting the logarithmic values of E_{50} from the three stress strain curves over the logarithm of K (Equation 2).
The exponentiation of the y-interception value of the regression line in Figure 10 gives the value of $E_{50,ref}$ and the slope of the line the power factor m.

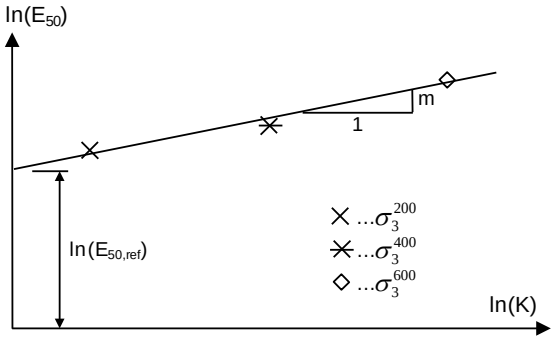

Figure 10: Determination of reference stiffness modulus $E_{50,ref}$ and exponent m

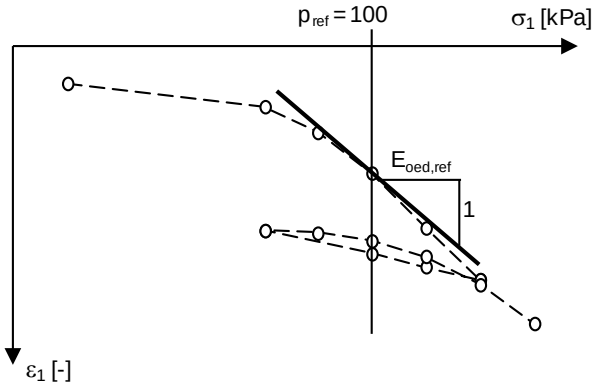

Figure 11: Determination of $E_{oed,ref}$ from oedometer test

The reference stiffness modulus for isotropic compression $E_{oed,ref}$ is defined as the tangential stiffness at $\sigma_1 = p_{ref} = 100$ kPa at primary loading from the oedometer test (Figure 11).

The dilation angle ψ is given by the gradient of the volumetric strain curve from drained triaxial tests and has its maximum at the point of peak shear stress [1], [11].

FEM analysis of Finstertal dam

Model parameters for Finstertal dam

The Hardening Soil parameters for the zones 2a, 2b, 2c and the remaining overburden (zone 5) were calibrated from triaxial and oedometer tests carried out by a maximum particle size of 31.5 mm and 20 mm, respectively. It is recognized from the calibration of the material parameters based on laboratory tests that the reference stiffness modulus $E_{50,\ ref}$ and $E_{ord,ref}$ are in the same order of magnitude. The reference modulus for unloading/reloading $E_{ur,ref}$ from triaxial tests amounts two to three times the value of $E_{50,ref}$. This is in accordance with findings from various publications [4], [5]. The determined material parameters for the numerical computation are listed in Table 3.

TABLE 3: HARDENING SOIL PARAMETERS ZONES 2A, 2B, 2C, 5

Zone	$E_{50,ref}$ [kN/m²]	$E_{oed,ref}$ [kN/m²]	$E_{ur,ref}$ [kN/m²]	m [-]	c [kN/m²]	φ [°]	Rf [-]	ψ [°]
2a	66300	66000	170000	0,53	145	41	0,49	5
2b	54180	52000	110000	0,34	58	43	0,75	4
2c	54180	52000	110000	0,34	58	43	0,75	4
5	28000	26000	70000	0,47	50	39	0,60	3

The material parameters R_f, $E_{50,ref}$ and m for the shell zones 3, 3a and 3b were determined from the stress strain curves pictured in Figures 5 and 6. Findings from the laboratory tests of zones 2a and 2b were the basis for the valuation of $E_{oed,ref}$ and $E_{ur,ref}$. The angle of dilation ψ was determined from triaxial tests on crushed orthogneiss. The set of parameters in Table 4 for the shell zones comprises: [A] values for the end of construction stage for the upstream (US) and downstream (DS) side with higher stiffness in the upstream zones 3, 3a due to positive effects from wetting, [B] values to model saturation settlements in the upstream rockfill due to grain breakage and redistribution of the particles after first reservoir filling/drawdown and [C] parameters to model the long-time behaviour of the embankment.

TABLE 4: HARDENING SOIL PARAMETERS ZONES 3, 3A AND 3B FOR VARIOUS STAGES

Zone	$E_{50,ref}$ [kN/m²]	$E_{oed,ref}$ [kN/m²]	$E_{ur,ref}$ [kN/m²]	m [-]	c [kN/m²]	φ [°]	Rf [-]	ψ [°]
[A] End of construction								
US 3,3a	84260	80400	170000	0,59	78	36	0,72	2
DS 3,3a	74170	70000	150000	0,47	57	37	0,70	2
3b	96740	94000	200000	0,59	82	36	0,73	3
[B] First reservoir filling/drawdown								
US 3,3a	80400	80400	175000	0,14	40	39	0,77	2
[C] 15 years of operation								
3,3a	66510	62000	145000	0,41	70	33	0,70	2
3b	82440	82000	167000	0,51	77	35,5	0,74	3

The best fit to laboratory tests on asphaltic concrete samples for the core membrane was obtained by using the standard Mohr-Coulomb model:

TABLE 5: MOHR-COULOMB PARAMETERS ZONE 1

Zone	E [kN/m²]	ν [-]	c [kN/m²]	φ [°]	ψ [°]
1	70000	0,489	420	30	8

The determined material parameters mentioned in Table 3 to 5 were validated by numerical single element tests.

Modelling of dam construction

The numerical analysis of Finstertal rockfill dam was carried out on the main dam cross section (Figure 1) using 15-node triangular elements. The boundaries were fixed on the base and vertical edges. The size of the model is at least three times the contact area in the length and two times the height of the dam. Starting with the virgin terrain, construction was simulated in 14 stages using the material parameters listed in Table 3, 5 and Table 4 [A].

By comparison of the results from the numerical computations with the measured data it was possible to evaluate the quality of the stress strain relations. For the end of construction stage the measured (effective) vertical stresses σ'_{yy} and horizontal stresses σ'_{xx} as well as the settlements u_y are compared with the results from the numerical analysis.

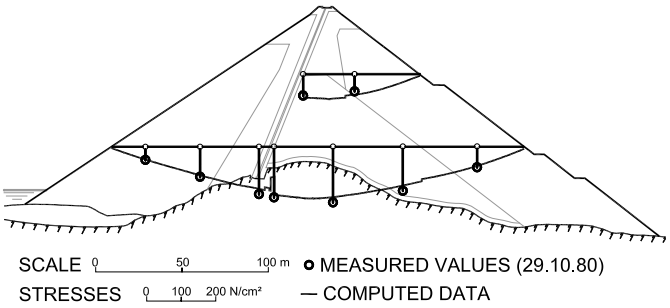

Figure 12: Vertical stresses σ'_{yy} along measuring sections at the end of construction

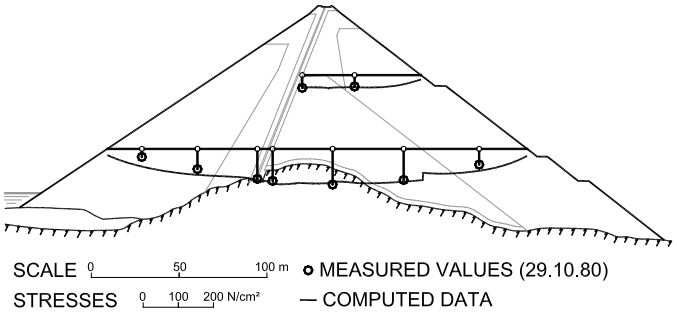

Figure 13: Horizontal stresses σ'_{xx} along measuring sections at the end of construction

The stresses σ'_{yy} and σ'_{xx} are plotted for two horizontal sections in which the measuring was carried out (Figure 12 and 13). The results from finite element computation indicate that the stress distribution is homogeneous along the path and the asphalt core has no great influence on the stress distribution. No stress redistributions occurred within the dam body due to the balanced stiffness characteristics of the dam zoning. The computed stresses fit the measured data very well with a maximum deviation from numerical results to measured data by 8%.

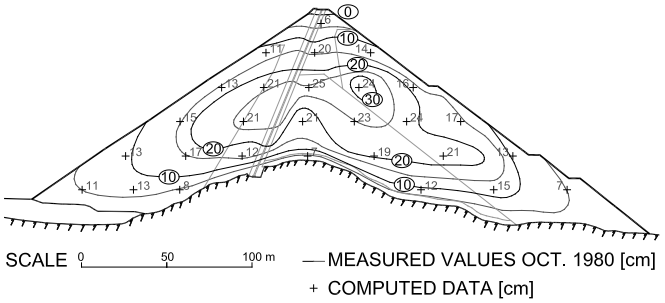

Figure 14: Settlements u_y in the dam at the end of construction

The maximum amount of settlement $u_{y,max}$ occurred in the downstream side of the dam and reached a value of 30 cm. Figure 14 compares the numerical computation (scatter plots) to the deformation pattern obtained from measurement (continuous lines). It can be seen that the distribution and the order of magnitude is in good accordance.

First reservoir filling

Filling of the reservoir was modelled in three stages until full supply level was reached. Effects from redistribution of soil particles due to saturation accompanied with potential of grain breakage were modelled by reducing stiffness and strength parameters for upstream zones 3, 3a (parameters Table 4 [B]). During impoundment the specific weight changes in the saturated part of the upstream zones due to hydrostatic uplift. The vertical stresses σ'_{yy} in the upstream shell zones decrease approximately 50% regarding to the end of construction stage. The additional load transfer from impoundment occurs over the downstream zone 3b made of well graded and compacted moraine material. The main stress axis rotate within this zone. The vertical stresses have their maximum in the near range of the core membrane and decrease progressional from the core to the downstream interface of zone 3b and 3a to a value similar to the end of construction stage (Figure 15).

The asphaltic concrete core acts as an impermeable membrane within the dam. Due to the load from impoundment this membrane is pushed towards the downstream side. The upstream zones doesn't come along with the horizontal movement of the core and as a reaction the effective horizontal stresses σ'_{xx} decrease in the upstream shell zones and relative displacements occur at the interface between the core and the upstream transition zone 2a. The effective horizontal stresses at the downstream side of the core have their maximum in the direct vicinity of the core and decrease steadily (Figure 16).

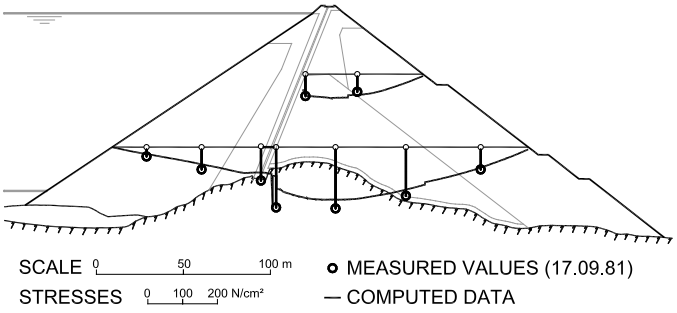

Figure 15: Vertical stresses σ'_{yy} along measuring sections at full supply level

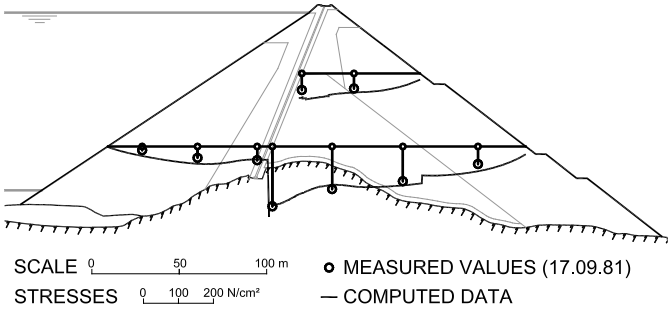

Figure 16: Horizontal stresses σ'_{xx} along measuring sections at full supply level

The measured horizontal displacement of the asphaltic core due to the impoundment of the reservoir is plotted in Figure 17 with its maximum of 14 cm at the crest. The results from numerical computation overestimate the horizontal displacements of the membrane by only 4 cm.

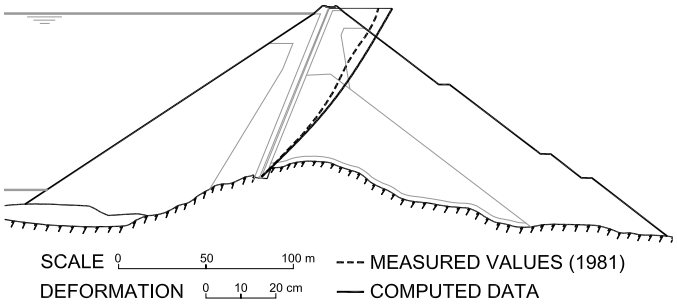

Figure 17: Horizontal displacement of the asphaltic concrete core along measuring sections at full supply level

Conclusion

Stress strain curves for shell zone material derived from measurements in existing dams and laboratory tests were used to calibrate the nonlinear Hardening Soil model. A two dimensional finite element calculation was carried out at the main dam cross section of Finstertal dam to evaluate the quality of this stress strain curves. The comparison of numerical results with the real deformations and stresses show that the stress strain curves for shell zone material are appropriate to describe the behaviour of Finstertal dam. An advanced procedure for calibration of the Hardening Soil parameters was required to display the stress strain curves adequately. No random fit procedure had to be applied at all. It could be proved that the determined material parameters can be used for analysis of dam behaviour, assuming that the fill density and lithology are similar to those at Finstertal dam.

References

[1] Atkinson J. (2007). *The Mechanics of soil and foundation,* Second edition, Taylor & Francis, New York.

[2] Duncan J. M., Chang C. Y. (1970). *Nonlinear analysis of stress and strain in soils,* Journal of the Soil Mechanics and Foundations Division, Vol. 96, No. 5, September/October 1970, pp. 1629-1653.

[3] Duncan J. M., Byrne P., Wong K., Mabry P. (1980). *Strength, stress-strain and bulk modulus parameters for finite element analysis of stresses and movements in soil masses,* Report No. UCB/GT/80-01, Department of civil engineering, University of California, Berkeley.

[4] Brinkgreve R. and Broere W. (2008). *Plaxis 2D – Version 9.0. Part 3: material models manual*. Delft. Netherlands.

[5] Schanz T., Vermeer P. A., Bonnier P. G. (1999). *The Hardening Soil model – formulation and verification.* In: Adachi, T., Oka, F., Yashima, A. (eds), Proc. Plaxis Symposium "Beyond 2000 in Computational Geotechnics", Amsterdam, Balkema, Rotterdam, 1999, pp. 281-296.

[6] Schwab. H. H. (1979). *Staudamm Gepatsch, Analysen zum langjährigen Verhalten 1962 – 1978.* Österreichische Wasserwirtschaft Heft 5/6, pp. 202-210.

[7] Schwab. H. H. (1984). *Analyse der Kontrollmessungen im Staudamm Finstertal*. Wasserwirtschaft 74 (1984), pp. 172-179.

[8] Schwab. H. H.. (1984). *Der 149 m hohe Staudamm Finstertal der Tiroler Wasserkraftwerke Aktiengesellschaft – Eine wissenschaftliche Analyse des Tragverhaltens*. Dissertation, University of Innsbruck 1984.

[9] Schmid R. (1992). *Das Tragverhalten von Erd- und Steinschüttdämmen mit Asphaltbeton-Kerndichtungen*, Berichte der Versuchsanstalt Obernach und des Lehrstuhls für Wasserbau und Wassermengenwirtschaft der Technischen Universität München, Nr. 70.

[10] Schober W. (1967). Behaviour of the Gepatsch rockfill dam, Commission Internationale des Grands Barrages, Istanbul, pp. 677 -699.

[11] Steinar N. (2008). Finite elements in geotechnical engineering, Norwegian University of Science and Technology, Geotechnical Division, Lecture Notes TBA 4115, Trondheim, Norway.